

Timescale Analysis of Spectral Lags

Ti-Pei Li^{1,2,3*}, Jin-Lu Qu², Hua Feng³, Li-Ming Song²,
Guo-Qiang Ding² and Li Chen⁴

¹ Department of Physics & Center for Astrophysics, Tsinghua University, Beijing

² Particle Astrophysics Lab., Inst. of High Energy Physics, Chinese Academy of Sciences

³ Department of Engineering Physics & Center for Astrophysics, Tsinghua University

⁴ Department of Astronomy, Beijing Normal University

Accepted 2004 June 18

Abstract A technique for timescale analysis of spectral lags performed directly in the time domain is developed. Simulation studies are made to compare the time domain technique with the Fourier frequency analysis for spectral time lags. The time domain technique is applied to studying rapid variabilities of X-ray binaries and γ -ray bursts. The results indicate that in comparison with the Fourier analysis the timescale analysis technique is more powerful for the study of spectral lags in rapid variabilities on short time scales and short duration flaring phenomena.

Key words: methods: data analysis — binaries: general — X-rays: stars — gamma rays: bursts — X-rays: bursts

1 INTRODUCTION

The analysis of spectral lag between variation signals in different energy bands is an important approach to get useful information on their producing and propagation processes in celestial objects. Observed intensity variations are usually produced by various processes with different time scales and different spectral lags. A lag spectrum, a distribution of time lags over Fourier frequencies, can be derived from two related time series with the aid of the Fourier transformation. Let $x(t_i)$ and $y(t_i)$ be two light curves observed simultaneously in two energy bands at times t_i , their Fourier transforms are $X(f_j)$ and $Y(f_j)$ respectively, and the cross spectrum $C(f_j) = X^*(f_j)Y(f_j)$. The argument of the cross spectrum $C(f_j)$ is the phase difference between the two processes at frequency f_j , or the time lag of photons in band 2 relative to that in band 1

$$\tau(f_j) = \arg[C(f_j)]/2\pi f_j . \quad (1)$$

The Fourier analysis technique has been most widely used in studying spectral lags.

The time domain method for studying spectral lags can be based on the correlation analysis. For two counting series $x(t_i)$, $y(t_i)$ (or $x(i)$, $y(i)$), the observed counts in the corresponding

* E-mail: litp@mail.tsinghua.edu.cn

energy band in the time interval (t_i, t_{i+1}) with $t_i = (i - 1)\Delta t$, the cross-correlation function (CCF) of the zero-mean time series at lag $k\Delta t$ is usually defined as

$$\text{CCF}(k) = \sum_i u(i)v(i+k)/\sigma(u)\sigma(v) \quad (k = 1, \pm 1, \dots) \quad (2)$$

with $u(i) = x(i) - \bar{x}$, $v(i) = y(i) - \bar{y}$, $\sigma^2(u) = \sum_i [u(i)]^2$ and $\sigma^2(v) = \sum_i [v(i)]^2$. With CCF the time lag can be defined as $\Lambda = k_m \Delta t$ where $\text{CCF}(k)/\text{CCF}(0)$ has maximum at $k = k_m$. Instead of a lag spectrum provided by Fourier analysis, the correlation technique gives only a single value Λ of time lag. To an understanding of a physical process occurring in the time domain, we need to know spectral lags at different timescales, i.e. a timescale spectrum $\Lambda(\Delta t)$.

We can not simply equate a Fourier period with the timescale and interpret a Fourier spectrum in the time domain as the timescale spectrum. For example, a Fourier power spectrum can not be interpreted as the distribution of variability amplitude vs. timescale. A sinusoidal process with frequency f has no Fourier power at any frequency except f , but it does not mean that no variation exists at timescales shorter than $1/f$. One can make lightcurves with time steps smaller than $1/f$ and find that non-Poissonian variations of intensities do exist in such lightcurves. In fact, a frequency analysis is based on a certain kind of time-frequency transformation. Different mathematically equivalent representations with different bases or functional coordinates in the frequency domain exist for a certain time series, a Fourier spectrum with the trigonometric basis does not necessarily represent the true distribution of a physical process in the time domain. It has to be kept in mind that a mathematical transform may distort physical information contained in the observational data. For correct understanding the real process, one has to invert results obtained through a time-frequency transform into the real physical space. It is usually not easy to complete such an inversion. A sinusoidal process is the simplest signal in the frequency domain, but a complex one in the time domain. The correct procedure to invert a Fourier power spectrum $p_f(f)$ into the timescale spectrum $p(\Delta t)$ in the physical space (the time domain) is

$$p(\Delta t) = \int p_f(f) p(\Delta t|f) \Delta t ,$$

where $p(\Delta t|f)$ is the timescale spectrum of a sinusoidal process with frequency f and unit amplitude, which is not a simple value or function and can not be derived from the Fourier analysis.

To understand a time process correctly, we have to make timescale analysis directly in the time domain and need to develop spectral analysis technique in the time domain without using the Fourier transform or other time-frequency transformation. A preliminary algorithm to modify the conventional cross-correlation technique was proposed by Li, Feng & Chen (1999). After then the algorithms to evaluate timescale spectra of power density, coherence, spectral hardness, variability duration, and correlation coefficient between two characteristic quantities were worked out (Li 2001), the modified cross-correlation technique is a part of the timescale analysis method in the time domain. Recently we have developed and completed the modified cross-correlation technique, improved its sensitivity and lag resolution significantly. This paper presents the timescale analysis technique of spectral lags and its application to analyzing space hard x-ray and γ -ray data. The general procedure of timescale analyzing and the modified cross-correlation function for spectral lag analysis in the time domain are introduced in §2. The technique has been applied to studying spectral lags of hard X-rays from X-ray binaries, γ -ray bursts and terrestrial γ -ray flashes, some examples are shown in §3. Relevant discussions are made in §4.

2 METHOD

2.1 Timescale Analysis

Temporal analysis is an important approach to study dynamics of physical processes in objects. Usually we take some quantities, e.g., power density (variation amplitude), spectral lag, and coherence etc., to characterize temporal property of observed light curves. The complex variability of high-energy emission shown in different time scales is a common character for X-ray binaries, super massive black holes and γ -ray bursts. The variability is caused by various physical processes at different timescales. It is not easy to study the variation phenomena on a given time scale. Large time bin used in calculation will erase the information on shorter time scales. And the analysis result with a short time bin reflects not only the variation property on the short time scale, but may also be affected by that on longer ones up to the total time period used in the calculation. The fact that a lightcurve with time step Δt does not include any information of variabilities at timescales shorter than Δt can be used as a foundation of timescale analysis. A set of lightcurves with different time steps Δt produced by rebinning the same originally observed data with a time resolution δt is the basic material in timescale analysis.

Usually the originally observed data for temporal analysis is a counting series $x(j; \delta t)$ ($j = 1, \dots$) with a time resolution δt . To study variability on a timescale

$$\Delta t = M_{\Delta t} \delta t, \quad (3)$$

we need to construct a new lightcurve with the time step Δt from the native series by combining its $M_{\Delta t}$ successive bins by

$$x(i; \Delta t) = \sum_{j=(i-1)M_{\Delta t}+1}^{iM_{\Delta t}} x(j; \delta t). \quad (4)$$

As the lightcurve $\{x(\Delta t)\}$ does not include any information about the variation on any timescale shorter than Δt , it is suitable for studying variability over the region of timescale $\geq \Delta t$.

Let Λ denote the quantity under study. The value $\Lambda(\Delta t)$ of the quantity at the timescale Δt can be seen as a function of the lightcurve $x(i; \Delta t)$

$$\Lambda(\Delta t) = f_{\Lambda}[\{x(\Delta t)\}]. \quad (5)$$

The key point in timescale analysis is to find a proper algorithm f_{Λ} to calculate the value of the studied quantity Λ at a certain timescale Δt .

The procedure (4) of binning the native series $\{x(\delta t)\}$ to get $\{x(\Delta t)\}$ with a larger time step $\Delta t = M_{\Delta t} \delta t$ is started from the first bin of $x(j = 1; \delta t)$. From the native lightcurve we can get $M_{\Delta t}$ different lightcurves with the same time step Δt

$$x_m(i; \Delta t) = \sum_{j=(i-1)M_{\Delta t}+m}^{iM_{\Delta t}+m-1} x(j; \delta t), \quad (6)$$

where the combination starts from the m th bin of the native series, the phase factor $m = 1, \dots, M_{\Delta t}$ (see the diagrammatic sketch Fig. 1).

For sufficiently using the information about variation on the timescale Δt included in the originally observed lightcurve, we can calculate the studied quantity $\Lambda(\Delta t)$ for each $\{x_m(\Delta t)\}$ and take their average as the resultant value

$$\Lambda(\Delta t) = \frac{1}{M_{\Delta t}} \sum_{m=1}^{M_{\Delta t}} f_{\Lambda}[\{x_m(\Delta t)\}]. \quad (7)$$

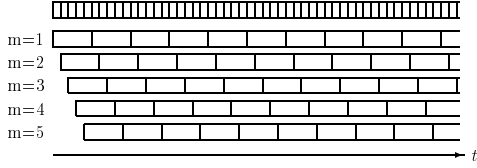


Fig. 1 From an originally observed time series with time resolution δt (schematically shown at the top where each small square represents a time bin with width δt) five different lightcurves with time step $\Delta t = 5\delta t$ can be constructed with different phase parameter m .

In timescale analysis the observed lightcurve $\{x(\delta t)\}$ is usually divided into L segments, each segment includes nearly equal number of successive bins. For each segment i , we can get a value $\Lambda_i(\Delta t)$ by Eq. (7), the average $\bar{\Lambda}(\Delta t)$ and its standard deviation $\sigma(\bar{\Lambda}(\Delta t))$ can be derived

$$\bar{\Lambda}(\Delta t) = \sum_{i=1}^L \Lambda_i(\Delta t) / L ,$$

$$\sigma(\bar{\Lambda}(\Delta t)) = \sqrt{\sum_{i=1}^L (\Lambda_i(\Delta t) - \bar{\Lambda}(\Delta t))^2 / L(L-1)} . \quad (8)$$

Usually we can use some convenient statistical methods based on the normal distribution to make statistical inference, e.g. significance test, on $\bar{\Lambda}(\Delta t)$. For the case of short time scale Δt , although the number of counts per bin may be too small for it to be assumed as a normal variable, it is easy from a certain observation period to get the total number L of segments large enough to satisfy the condition for applying the central limit theorem in statistics and using the normal statistics for the mean $\bar{\Lambda}(\Delta t)$.

2.2 Modified Cross Correlation Function

In timescale analysis for spectral lags, the observed data are two related counting series $\{x(i; \delta t)\}$ and $\{y(i; \delta t)\}$ in two energy bands with time resolution δt . If the timescale Δt under study is larger than the time resolution, we need to construct two new lightcurves, $\{x(i; \Delta t)\}$ and $\{y(i; \Delta t)\}$, by re-binning the originally observed series with the time step Δt . With the traditional CCF defined by Eq. (2), we can calculate the time lag Λ only if $\Lambda > \Delta t$. But for many physical processes the real time lag is shorter or even much shorter than the process timescale. For the purpose of applying correlation analysis to the general case of lag analysis, a modified CCF at lag $k\delta t$ has been proposed (Li, Feng & Chen 1999)

$$\text{MCCF}_0(k; \Delta t) = \sum_i u_1(i; \Delta t) v_{k+1}(i; \Delta t) / \sigma(u)\sigma(v) , \quad (9)$$

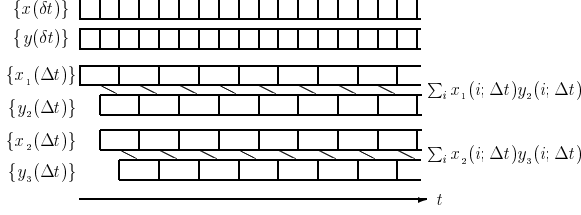


Fig. 2 MCCF of two native time series $\{x(\delta t)\}$ and $\{y(\delta t)\}$ at a time lag $\tau = \delta t$ ($\tau = k\delta t$, $k = 1$) and on a timescale $\Delta t = 2\delta t$. $\text{MCCF}(k = 1; \Delta t) = \frac{1}{2}[\sum_i x_1(i; \Delta t)y_2(i; \Delta t) + \sum_i x_2(i; \Delta t)y_3(i; \Delta t)]$

where the time step $\Delta t = M_{\Delta t}\delta t$, $\{u_k(\Delta t)\}$ and $\{v_k(\Delta t)\}$ are the zero-mean series of $\{x_k(\Delta t)\}$ and $\{y_k(\Delta t)\}$ respectively, and

$$\begin{aligned} x_m(i; \Delta t) &= \sum_{j=(i-1)M_{\Delta t}+m}^{iM_{\Delta t}+m-1} x(j; \delta t) , \\ y_m(i; \Delta t) &= \sum_{j=(i-1)M_{\Delta t}+m}^{iM_{\Delta t}+m-1} y(j; \delta t) . \end{aligned} \quad (10)$$

The lag resolution of CCF defined by Eq. (2) is Δt , and that of MCCF_0 defined above is the original time resolution δt .

For sufficiently using the information contained in the observed lightcurve, we propose to improve the definition of MCCF_0 further by following the procedure described by Eq. (7). The new and complete definition of MCCF at lag $k\delta t$ is

$$\begin{aligned} \text{MCCF}(k; \Delta t) &= \\ \frac{1}{M_{\Delta t}} \sum_{m=1}^{M_{\Delta t}} \sum_i u_m(i; \Delta t)v_{m+k}(i; \Delta t) / \sigma(u)\sigma(v) \end{aligned} \quad (11)$$

where $u_m(i; \Delta t) = x_m(i; \Delta t) - \bar{x}_m(\Delta t)$, $v_m(i; \Delta t) = y_m(i; \Delta t) - \bar{y}_m(\Delta t)$, $\bar{x}_m(\Delta t)$ and $\bar{y}_m(\Delta t)$ are the current averages for the used segments of lightcurve $\{x\}$ and $\{y\}$ respectively. The procedure of calculating a modified cross-correlation coefficient is schematically shown by Fig. 2. We can find a value k_m of k to satisfy the condition

$$\text{MCCF}(k = k_m; \Delta t) / \text{MCCF}(0; \Delta t) = \max , \quad (12)$$

then the lag of band 2 relative to band 1 on timescale Δt

$$\Lambda(\Delta t) = k_m \delta t . \quad (13)$$

For an observed time series $x(j; \delta t)$ with time resolution δt , we can similarly define a modified auto-correlation function at lag $k\delta t$ on timescale $\Delta t = M_{\Delta t}\delta t$

$$\begin{aligned} \text{MACF}(k; \Delta t) &= \\ \frac{1}{M_{\Delta t}} \sum_{m=1}^{M_{\Delta t}} \sum_i u_m(i; \Delta t)u_{m+k}(i; \Delta t) / \sigma^2(u) \end{aligned} \quad (14)$$

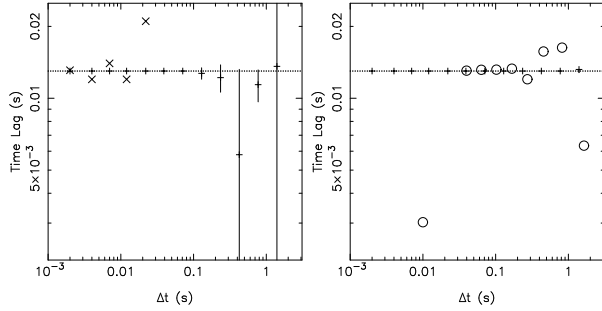


Fig. 3 Time lag vs. time scale of two white noise series with 13 ms time lag shown by the dotted horizontal line. *Left panel*: *Cross* – CCF lag; *Plus* – lag evaluated by MCCF_0 [Eq.(9)]. *Right panel*: *Circle* – lag from Fourier analysis; *Plus* – lag by MCCF [Eq.(11)].

where the $u_m(i; \Delta t) = x_m(i; \Delta t) - \bar{x}$, $x_m(i; \Delta t) = \sum_{j=(i-1)M_{\Delta t}+m}^{iM_{\Delta t}+m-1} x(j; \delta t)$. The FWHM of $\text{MACF}(\tau; \Delta t)$ can be taken as a measure of the duration of variation on time scale Δt . With MACF we can study the energy dependence of average shot width in a random shot process on different time scales.

2.3 Simulations

2.3.1 Poissonian signals

To compare the above MCCF technique of estimating time lags with the traditional CCF technique and Fourier analysis, we produce two photon event series of length 1000 s with a known time lag between them. The series 1 is a white noise series with average rate 200 cts s^{-1} and series 2 consists of the same events in series 1 but each event time is delayed 13 ms. Besides the signal photons mentioned above, the two series are given independent additional noise events at average rate 300 cts s^{-1} . By binning the two event series, two light curves with time resolution $\delta t = 1$ ms are produced. We make time lag analysis at timescales Δt from 1 ms to 2 s for the two lightcurves by CCF, MCCF and Fourier analysis techniques separately (in Fourier analysis we use Fourier cross spectrum with 1 ms light curves and 4096-point FFT and take Fourier frequency $f = 1/\Delta t$), the results are shown in Fig. 3. In the left panel of Fig. 3, the cross signs show lags derived by CCF and plus signs by MCCF_0 defined by Eq. (9). For the timescale region of Δt shorter or approximately equal to the magnitude of the true lag 0.013 s where CCF works, MCCF_0 can provide more reliable results with better accuracy. The circles in the right panel of Fig. 3 indicate the Fourier lags, for the short timescale region of $\Delta t \lesssim 0.3$ s (or high frequency region of $f \gtrsim 30$ Hz) the Fourier analysis can not give any meaningful result.

In the timescale region of $\Delta t \gtrsim 0.1$ s, the estimates of time lag by MCCF_0 defined by Eq. (9) (plus signs in the left panel of Fig. 3) show significant fluctuation about the expectation. We use the improved MCCF defined by Eq. (11) to calculate the lag spectrum again, the plus signs in the right panel of Fig. 3 indicate the result. Comparing the lag spectra with MCCF_0 [Eq. (9)] and MCCF [Eq. (11)], plus signs in the left panel and right panel of Fig. 3, we can see that using the improved MCCF can improve the lag spectrum significantly in the large timescale region.

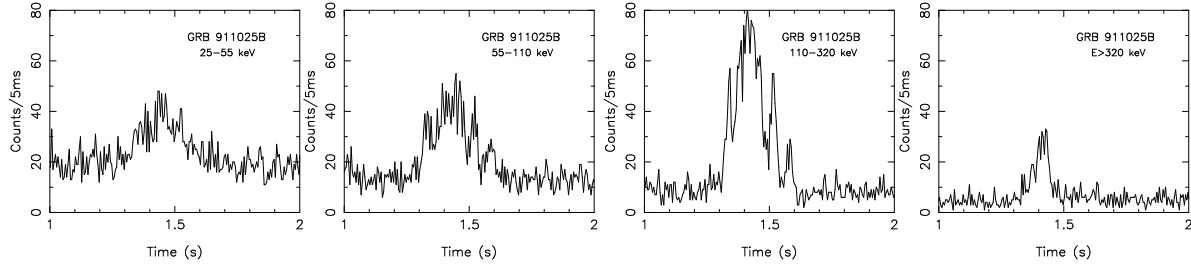


Fig. 4 Light curves of a γ -ray burst GRB 911025B observed by BATSE in channels 25-55 keV, 55-110 keV, 110-320 keV, and > 320 keV, separately.

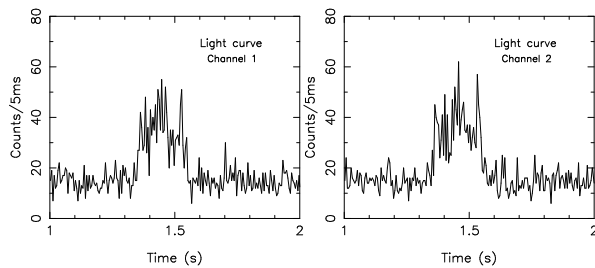


Fig. 5 Simulated light curves for two channels. The burst process for channel 2 is delayed 0.01 s to channel 1.

2.3.2 Transient signals

To study the relative timing of transient emission at different energies is a difficult task in astrophysics. Neither the Fourier analysis nor the traditional cross-correlation technique can get meaningful result of spectral lags from the observed data of short γ -ray bursts. We show here the ability of MCCF to study spectral lags in prompt emission of short γ -ray bursts by simulation. Fig. 4 shows light curves with 5 ms time bin observed by BATSE on *CGRO* mission for a γ -ray burst, GRB 911025B (BATSE trigger number 936), in channel 25-55 keV, 55-110 keV, 110-320 keV, and > 320 keV, respectively. The time-tagged event (TTE) data of BATSE contains the arrival time ($2\mu\text{s}$ resolution) of each photon for the short duration burst GRB 911025B. In our simulation, we use the 25-55 keV photons between 1.35 s and 1.55 s in the TTE data as the burst events in channel 1. The burst events in channel 2 are the same in channel 1 but each time is delayed 0.01 s. By binning the two event series with time bin 5 ms, expected signal series in channel 1 and 2 are produced. Two simulated lightcurves in channel 1 and 2 are generated by taking random samples from the expected signal series and adding independent background noise at the average of 15 counts each bin, shown in Fig. 5.

From the two simulated lightcurves we use MCCF to calculate the time lags at timescale $\Delta t = 0.005$ s, 0.015 s, 0.045 s, 0.14 s, and 0.43 s separately, the results are shown in Fig. 6. The error bar of time lag at each timescale is estimated from 200 bootstrap samples. The simulation result indicates that MCCF is a useful tool in relative timing of transient processes.

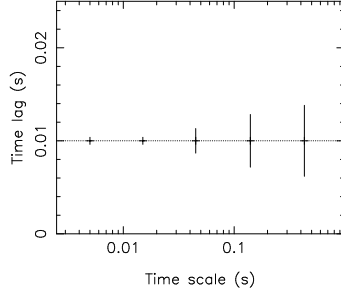


Fig. 6 Time lag vs timescale of two simulated light curves in Fig. 5. *Dotted line* – expected time lag. *Cross* – measured by MCCF.

2.3.3 Timescale dependent process

Spectral time lags observed for X-ray binaries and AGNs are usually timescale dependent. For example, the Fourier lag between 14.1-45 keV and 0-3.9 keV of X-ray emission from Cyg X-1 in the low state continuously varies with Fourier frequency, from ~ 30 ms at 0.1 Hz decreasing down to ~ 2 ms at 10 Hz (Nowak et al 1999). Real data in timing can be seen as a complex time series with multiple timescale components. The timescale dependence of spectral lags can be the intrinsic property of the emission process and/or come from different processes dominating at different timescales. Correctly detecting the timescale dependence of spectral lags is important to studying the undergoing physical processes. Now we compare the abilities of MCCF and Fourier technique to study spectral lags of time series with multiple timescale components. Two light curves of a complex process consisting of five independent random shot components are produced by Monte Carlo simulation. Each signal component i ($i = 1 - 5$) consists of random shots with shape of profile $a \cdot \exp[-(t - t_0)/\tau_i]^2$, where the peak height a is randomly taken from the uniform distribution between zero and the maximum. The separation between two successive shots is exponentially distributed with average separation τ_i . For each component i , we produce a 3000 s counting series of band 1 with a step of $\delta t = 1$ ms and average rate 200 cts s^{-1} . The corresponding series in band 2 consists of the same events in series 1 but each event time is delayed Λ_i s. The characteristic time constants τ_i of the five signal components are 0.005, 0.01, 0.02, 0.04, and 0.08 s, and their time lags are 0.004, 0.008, 0.012, 0.016, and 0.02 s respectively. Summing up the five series for each band, we produce two expected signal lightcurves. Two synthetic light curves with time step 1 ms are made by random sampling the expected light curves with Poisson fluctuation plus a independent white noise at mean rate of 100 cts s^{-1} . For the two light curves, we use their Fourier cross spectrum and 4096-point FFT and MCCF in the time domain to calculate the time lags on different time scales Δt and show the results in Fig. 7.

To derive the expected lag spectrum of the above synthetic lightcurves, we calculate the timescale distribution of power density for each shot component using the algorithm of estimating power density spectrum $p(\Delta t)$ in the time domain (Li 2001; Li & Muraki 2002). As an example, Fig. 8 shows the distribution of variation power $p(\Delta t)\Delta t$ (rms²) vs. time scale Δt for the expected light curve of the shot process with $\tau = 0.01$ s. As shown in Fig. 8, an individual shot component with characteristic time τ_i has its variation power distributed over a certain time scale region. The time lag between two bands should appear in the whole timescale region where the signal variation power exists. The expected lag of the two synthetic light curves with multiple components on timescale Δt should be estimated as a weighted average of five lags Λ_i

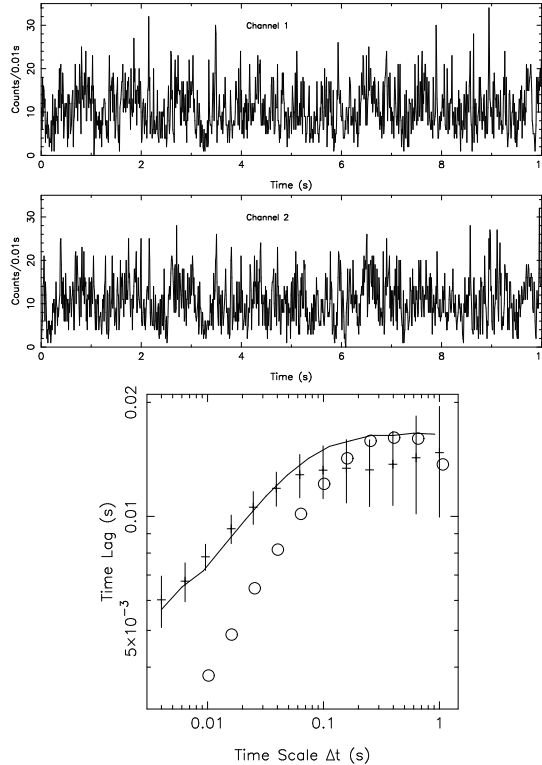


Fig. 7 *Top and Middle:* Synthetic lightcurves with time bin 0.01 s for a complex process consisting of different characteristic timescales and different spectral lags. *Bottom:* Timescale spectra of time lag; *Solid line* – the expected lag spectrum, *Plus* – MCCF lag, *Circle* – lag from Fourier analysis.

of individual component with corresponding weight factor $p_i(\Delta t)\Delta t$

$$\Lambda(\Delta t) = \sum_i p_i(\Delta t)\Delta t \cdot \Lambda_i \quad (15)$$

The solid line in Fig. 7 is the expected lag distribution calculated by Eq. (15). We can see from Fig. 7 that the Fourier cross spectrum fails to detect lags in the short timescale region, but MCCF works well. More simulations with different signal to noise ratios show that the MCCF technique is capable of correctly detecting time lags from severely noisy data and the inefficiency of detecting time lag in short time scale region is an intrinsic weakness of the Fourier technique, even for data with much higher signal to noise ratio the Fourier analysis still can not detect lags in the high frequency region.

3 APPLICATIONS

The timescale spectral method for time lag analysis is a powerful tool in revealing the characteristic of emission process in objects. With the help of MCCF technique, as a example, we can judge between different production models of x-rays from accreting black holes. The energy spectra of hard X-rays from black hole binaries can be fitted well by Comptonization of

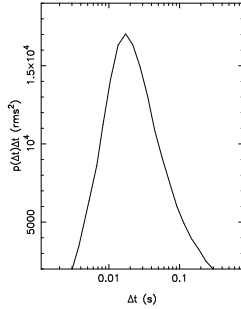


Fig. 8 Power distribution $p(\Delta t)\Delta t$ vs. time scale Δt of a random shot process with a characteristic timescale $\tau = 0.01$ s, where $p(\Delta t)$ (rms^2/s) is the power density on the timescale Δt of the process.

soft photons by hot electrons in the vicinity of the compact sources. To explain the observed energy spectra the uniform corona model was suggested initially (Payne 1980), in which the soft photons from the central region of the system are Comptonized by the hot electrons of corona. The Comptonization process makes the observed hard photons undergo more scattering than the low energy photons and therefore the hard photons are naturally delayed from soft photons. Hard lags are not correlated with the variability timescale (or variability frequency) in the uniform corona model, but later study show strong timescale-dependence of time lags (Miyamoto & Kitamoto 1988). For overcoming the contradiction between prediction by the uniform corona model and observed results, other models, such as the non-uniform corona model (Kazanas et al 1997), the magnetic flare model (Poutanen & Fabian 1999) and the drifting-blob model (Böttcher & Liang 1999) are proposed. The hard X-ray lags are studied by observations with PCA detector on board *RXTE* mission in using the Fourier technique to the black hole candidate Cyg X-1 in the low state (Nowak et al 1999), high state (Cui et al 1997a), and during spectra transitions (Cui et al 1997b). The meaningful Fourier spectra of time lag from PCA/*RXTE* data are all limited in the range of Fourier frequency $\lesssim 30$ Hz (or timescale $\gtrsim 0.03$ s) and, except that with a uniform corona, all models mentioned above can fit the observed lag spectra of Cyg X-1. To test these models, we need to compare the expected and observed lags in the higher frequency range or on the shorter time scales.

Kazanas et al (1997) present that for the PCA/*RXTE* observation of June 16 1996 (ObsID P10512), hard X-ray time lags of Cyg X-1 in the soft state as a function of Fourier frequency over the region of 8 - ~ 30 Hz can be well fitted by the non-uniform corona model. From the same data, we measure the time lags between 13-60 keV and 2-5 keV on short time scales down to $\Delta t \sim 1$ ms with MCCF and the results, shown in the left panel of Fig. 9, can not be fitted by this model (the solid line in the figure). The drifting-blob model (Böttcher & Liang 1999) also can explain the observed time lags in the Fourier period region above 0.1 s. On short time scales, the Comptonization process of the drifting-blob model is similar with that of the non-uniform corona model. Thus the time lag will have similar time scale dependence, i. e. time lag will decrease with time scale as quickly as the behavior of non-uniform corona model on short time scales. The drifting blob model also can not explain the observed time lags of Cyg X-1 on the short time scales.

Poutanen & Fabian (1999) propose the magnetic flare avalanche model to explain the observed time lags of Cyg X-1, and parameterize the spectral evolution of a magnetic flare and the avalanche process based on the PCA/*RXTE* observation on October 23 1996 (ObsID P10241).

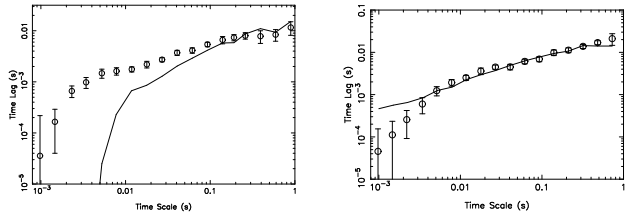


Fig. 9 Hard X-ray time lag vs. time scale of Cyg X-1. *Left panel:* Circle – time lag between 13 - 60 keV and 2 - 5 keV in the soft state of Cyg X-1 on 1996 June 17 (PCA/RXTE ObsID P10512) measured by MCCF; *Solid line* – expected by the non-uniform corona model. *Right panel:* Circle – lags between 13 - 60 keV and 2 - 5 keV of Cyg X-1 in the hard state on 1996 October 23 (PCA/RXTE ObsID P10241) measured by MCCF; *Solid line* – lags between 27 keV and 3 keV predicted by the magnetic flare model.

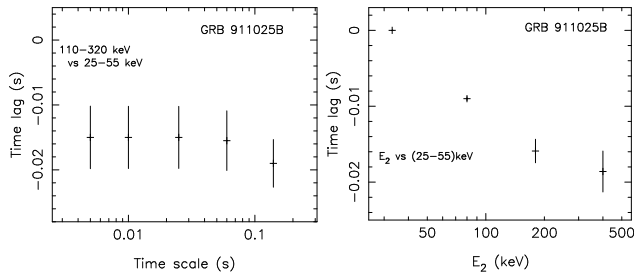


Fig. 10 Hard lags of GRB 911025B measured by MCCF. *Left panel:* Timescale spectra of time lag of (110-320) keV vs. (25-55) keV. *Right panel:* Energy dependence of time lag of hard photons vs. (25-55) keV, averaged for timescales 0.005 s, 0.01 s, 0.25 s, 0.06 s, and 0.14 s.

In the right panel of Fig. 6, we show the measured time lags with the observation data and MCCF technique (the circles) and the predicted by the model (the solid line). The predicted time lags can fit the measured time lags well in the time scales range between ~ 4 ms and 1 s, much better than other models, although there seems to be overestimated on the shortest timescales. This example shows that the capability of MCCF for detecting time lags on short time scales can help us to reveal the underlying physics in high energy process in objects.

The MCCF is particularly useful in studying transient processes. The BATSE detector has discovered an unexplained phenomenon: a dozen intense flashes of hard X-ray and γ -ray photons of atmospheric origin (TGFs) (Fishman et al 1994). As all the observed TGFs were of short duration (just a few milliseconds), it is difficult to study their temporal property by conventional techniques. With the aid of the preliminary MCCF (MCCF₀, Eq. (9) in this paper), Feng et al. (2002) reveal that for all the flashes with high signal to noise ratio γ -ray variations in the low energy band of 25 - 110 keV relative to the high energy band of > 110 keV are always late in the order of $\sim 100 \mu\text{s}$ in the timescale region of $6 \times 10^{-6} - 2 \times 10^{-4}$ s and pulses are usually wide. The above features of energy dependence of time profiles observed in TGFs support models that TGFs are produced by upward explosive electrical discharges at high altitude.

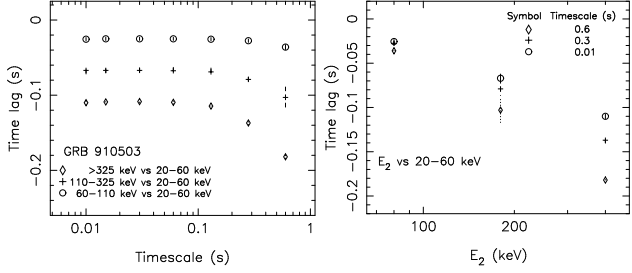


Fig. 11 Hard lags of GRB 910503 measured by MCCF. *Left panel:* Timescale spectra of time lag. *Circle* – (20-60)keV vs. (60-100)keV; *Plus* – (20-60)keV vs. (110-325)keV; *Diamond* – (20-60)keV vs. > 325keV. *Right panel:* Time lag of 20-60 keV photons vs. energy of hard photons. *Circle* – timescale 0.01 s; *Plus* – timescale 0.3 s; *Diamond* – timescale 0.6 s.

Efforts have been made to measure the temporal correlation of two GRB energy bands by the CCF technique (e.g. Link, Epstein & Priedhorsky 1993; Cheng et al 1995; Wu & Fenimore 2000; Norris 2002). The CCF technique has no necessary sensitivity to make timing analysis for weak events. For strong bursts the DISCSC data in BATSE database, 4-channel light curves with 64 ms time resolution, are usually analyzed, but it fails with the traditional ACF and CCF in the case that the existed spectral lags comparable or smaller than 64 ms whatever how strong the burst is. For short bursts of duration < 2 s, we can use TTE data to construct high resolution lightcurves, as the four lightcurves of time resolution $\delta t = 5$ ms for GRB 911025B shown in Fig. 4. We failed to get statistically meaningful results in spectral lag analysis for short GRBs by using CCF and $MCCF_0$. The MCCF technique can help us to reveal spectral lags in strong short bursts. As an example, with the lightcurves of GRB 9110258B and MCCF, we calculate the time lag between two channels at timescale $\Delta t = 0.005$ s, 0.01 s, 0.025 s, 0.06 s, and 0.14 s respectively. In our calculation only partial data having higher signal to noise ratio recorded during 1.29 s and 1.62 s is used. The obtained timescale spectrum and energy dependence of time lags are shown in Fig. 10. For long γ -ray bursts, the BATSE Time-to-Spill (TTS) data record the time intervals to accumulate 64 counts in each of four energy channels. The TTS data have fine time resolution than 64 ms of DISCSC data when the count rate is above 1000 cts s^{-1} . The TTS data can be binned into equal time bins with a resolution of $\delta t \sim 10$ ms and our simulations show that from the derived lightcurves the temporal and spectral properties with the time resolution δt can be reliably studied with MCCF for typical GRBs recorded by BATSE. As an example, the left panel of Fig. 11 shows the lag spectrum of GRB 910503 detected by BATSE with a duration ~ 50 s. From the MCCF lag spectra, we can further derive the energy dependence of lag at different timescales, shown in the right panel of Fig. 11. The results shown in Figs. 10 and 11 indicate that MCCF can be used to explore temporal and spectral properties for both long and short γ -ray bursts.

4 DISCUSSION

The technique for timescale analysis with MCCF is developed from the standard cross correlation function CCF. For determining CCF from unevenly sampled data which are common in astronomical contexts, several different methods have been introduced, i.e., interpolating the data between observed points to form a continuous function (Gaskell & Sparke 1986), the discrete correlation function (DCF, Edelson & Krolik 1988), evaluating CCF with the dis-

crete Fourier transform (Scargle 1989), and z-transformed discrete correlation function (ZDCF, Alexander 1997). Introducing MCCF was motivated by the need of improving the resolution and sensitivity of the standard correlation analysis. Comparing the two definitions, Eq. 11 for MCCF and Eq. 2 for CCF, we can see that MCCF includes more information from the observed data than CCF does. That the lag $\tau = k\delta t$ in MCCF has the same resolution with the originally observed data but the resolution of CCF lag is Δt and that MCCF is calculated by summing over $m = 1, 2, \dots, M_{\Delta t}$ (using all possible lightcurves that can be derived from the native data with timescale Δt) but CCF only uses one lightcurve for a given time bin Δt – make MCCF has better resolution and sensitivity in measuring spectral lags.

Three different temporal quantities exist in the timescale analysis: time t , time resolution δt , and time scale Δt . The originally observed data, based on which both the frequency analysis and timescale analysis are performed, is time series $x(t)$ in the time domain with a time resolution δt . With frequency analysis, we can derive a frequency spectrum $\Lambda(f)$ for a studied characteristic quantity Λ (in this paper Λ is time lag, in other spectral analysis it may be power density, coherence, or other quantity) from the observed time series. In frequency analysis, the observed time series has to be transformed into the frequency domain first with the aid of time-frequency transformation, e.g. the Fourier transform, and the maximum frequency is determined by the time resolution δt . The timescale analysis is performed directly in the time domain without any time-frequency transformation. With timescale analysis we can derive a timescale spectrum $\Lambda(\Delta t)$ for the studied quantity Λ where the argument Δt , the variation timescale, is a variable similar to the frequency f in frequency analysis. The minimum timescale in timescale analysis is the time resolution δt of the originally observed data. To study temporal property on a certain timescale Δt , the used light curves should have a time step equal to the timescale under study. With MCCF we can measure any lag greater than the time resolution of observation at any given timescale and produce a timescale spectrum of time lags.

There exist two kinds of spectral analysis: frequency analysis and timescale analysis. Although the Fourier method is a common technique to make spectral analysis, it can not replace the timescale analysis in the time domain. As any observable physical process always occurs in the time domain, a frequency spectrum obtained by frequency analysis needs to be interpreted in the time domain. But a frequency analysis is dependent on a certain time-frequency transformation. A Fourier spectrum by using Fourier transform with the trigonometric basis does not necessarily represent the true distribution of a physical process in the time domain. The rms variation vs. timescale of a time-varying process may differ substantially from its Fourier spectrum, as an example, the Fourier spectrum of a random shot series significantly underestimates the power densities at shorter timescales (Li & Muraki 2002). The present work shows that, like Fourier power spectra, Fourier lag spectra also always significantly underestimate time lags at short timescales. The timescale analysis performed directly in the time domain can derive real timescale distribution for quantities characterizing temporal property. In comparison with the Fourier technique, timescale spectra of power density and time lag from the timescale analysis can more sensitively reveal temporal characteristics at short timescales for a complex process.

Welsh (1999) pointed out that the lag determined from the CCF should be considered only a characteristic time scale. Care has to be taken in interpreting measured lags with a particular physical model. Most techniques in timing can only treat timescale just in a synthetic meaning. For example, a correlation function lag of two shot series may caused not only by a time displacement between the two series, but also by changes in shot shape and intervals between two successive shots. Distinguishing different kinds of timescale and physical process is obviously helpful to study physics, that should be a goal in future development of time domain technique. Using a single analysis technique alone is often difficult to definitely distinguish the possible

processes and compiling different results of analysis from different view angles will be helpful. In comparison with the Fourier technique, the time domain technique has the freedom of choosing a proper statistic for a particular purpose. Recently Feng, Li & Zhang (2004) introduced a statistic $w(\Delta t)$ to study widths of random shots and diagnosed black hole and neutron star X-ray binaries by timing with the new designed statistic.

Acknowledgements This work is supported by the Special Funds for Major State Basic Research Projects and the National Natural Science Foundation of China. The data analyzed are obtained through the HEASARC on-line service provided by the NASA/GSFC.

References

- Alexander T. 1997, in: *Astronomical Time Series*, eds. D. Maoz, A. Sternberg, and E.M. Leibowitz (Dordrecht: Kluwer), 163
- Böttcher M., Liang E.P. 1999, *ApJ*, 511, L38
- Cheng L.X., Ma Y.Q., Cheng K.S., Lu T. & Zhou Y.Y. 1995, *A&A*, 300, 746
- Cui W., Heindl W.A., Rothschild R.E., et al. 1997a, *ApJ*, 474, L57
- Cui W., Zhang S.N., Focke W., & Swank J.H. 1997, *ApJ*, 484, 383
- Edelson R.A. & Krolik J.H. 1988, *ApJ*, 333, 646
- Feng H., Li T.P., Wu M., Zha M. & Zhu Q.Q. 2002, *Geophys. Res. Lett.*, 29, 6
- Feng H., Li T.P. & Zhang S.N. 2004, *ApJ*, 606, 424
- Fishman G. J. et al. 1994, *Science*, 264, 1313
- Gaskell C.M. & Sparke L.S. 1986, *ApJ*, 305, 175
- Hua X.M., Kazanas D. & Titarchuk L. 1997, *ApJ*, 482, L57
- Kazanas D., Hua X.M. & Titarchuk L. 1997, *ApJ*, 480, 735
- Lewin W.H.G., van Paradijs J., & van der Klis M. 1988, *Space Sci. Rev.*, 46, 273
- Li T. P., Feng Y.X. & Chen L. 1999, *ApJ*, 521, 789
- Li T. P. 2001, *Chin. J. Astron. Astrophys.*, 1, 313 (astro-ph/0109468)
- Li T. P. & Muraki Y. 2002, *ApJ*, 578, 374
- Link B., Epstein R.I., & Peiedhorsky W.C. 1993, *ApJ*, 408, L81
- Miyamoto S., & Kitamoto S. 1988, *Nature*, 336, 450
- Norris J.P., 2002, *ApJ*, 579, 386
- Nowak M.A., Wilms J., Vaughan B.A., Dove J.B., & Begelman C. 1999, *ApJ*, 510, 874
- Payne D.G. 1980, *ApJ*, 86, 121
- Poutanen J. & Fabian A.C. 1999, *MNRAS*, 306, L31
- Scargle J.D. 1989, *ApJ*, 343, 874
- van der Klis M. 1995, in *X-ray Binaries*, ed. Lewin W.H.G., van Paradijs J., van den Heuvel E.P.J., (London: Cambridge University Press), 252
- Welsh W.F. 1999, *PASP*, 111, 1347
- Wu B.B. & Fenimore E. 2000, *ApJ*, 535, L29